Competition between deep impurity and dopant behavior of Mg in GaN Schottky diodes

M. Schmeits,[a] N. D. Nguyen, and M. Germain
Institute of Physics, University of Liège, B4000 Sart-Tilman/Liège, Belgium

(Received 18 July 2000; accepted for publication 13 November 2000)

The effect of the deep acceptor Mg on the electrical characteristics of *p*-doped GaN Schottky diodes is analyzed. The theoretical study is based on the numerical resolution of the basic semiconductor equations, including the continuity equation for the Mg-related acceptor level. It gives the steady-state and small-signal analysis of *p*-doped GaN:Mg Schottky diodes, yielding as final result the frequency dependent capacitance and conductance of the structure. It is shown that the low-frequency characteristics are determined by the carrier exchange between the Mg related impurity level and the valence band, whereas above the impurity transition frequency, the hole modulation of the depletion layer edge governs the electrical response. Detailed results are shown on the effect of temperature, applied steady-state voltage and series resistance. The study of two back-to-back connected GaN Schottky diodes reveals the appearance of typical features in the electrical characteristics, depending on the respective Schottky barrier height of the two junctions.
 [DOI: 10.1063/1.1339208]

I. INTRODUCTION

The wide-gap semiconductor gallium nitride has received much attention during the past decade. It is considered as a basic material for visible and UV light emitters and UV visible blind detectors.[1–4] GaN-based bipolar junction transistors and heterojunction field effect transistors are another potential application field.[5,6]

The need for both *n*-type and *p*-type dopants for the realization of practical structures has led to active research to find the most efficient atomic impurities. For wide-gap semiconductors like SiC and GaN, Si is used as shallow *n* dopant. However, shallow *p* dopants do not exist. Rapid progress was obtained when *p*-type conduction by Mg doping with appropriate posttreatment was achieved. Magnesium is considered as a deep dopant with activation energies given in the literature in the range of 120–250 meV, the most frequently cited values being around 150–170 meV.[7–9] We label the total Mg concentration N_t and n_t is the concentration of occupied Mg levels.

With these values of the acceptor ionization energy, Mg acts simultaneously as a dopant and as a deep impurity. Shallow dopants are considered as fully ionized, at least for all temperatures of practical interest. The Mg acceptor level is only partially ionized for these temperature ranges. At thermal equilibrium, its occupation is fixed by the relative position of the defect level with respect to the Fermi energy. This in turn results from the charge neutrality condition, which contains the ionized acceptor charge qn_t as one of its terms. Mg acts as dopant, providing free holes for the valence band, but less than the total Mg concentration. In a junction, at the depletion layer edge, the hole concentration varies from zero to a maximum value, which is the total acceptor concentration in the case of shallow dopants but which is less in the case of Mg doping. This influences the contribution of the modulation of the depletion layer edge to the total junction capacitance.

When used in a *p–n* junction or in a metal/GaN-*p* Schottky diode, the Mg-related acceptor level may cross the hole quasi-Fermi level. The modulation of the applied voltage modifies the occupation of the Mg-related energy level and gives rise to typical features in the electrical characteristics. This behavior is similar to that of deep impurities,[10–12] but with the difference that the crossing point here separates regions where the concentration of the occupied levels is respectively N_t and n_t, i.e., the impurity levels are totally ionized and partially ionized. In the classical deep impurity case, however, these concentrations are, respectively, N_t and zero.

As the value of n_t is strongly temperature dependent, important effects in the study of electrical characteristics as a function of temperature can be expected. We will effectively show that this is the case and that moreover, in the resulting response to an applied voltage modulation, there is a competition between the contribution of the modulated defect state population and the hole concentration at the depletion layer edge. For low frequencies, in the classical deep impurity context, both act simultaneously and independently. In the deep dopant case however we will show that, at low frequencies, the holes provided by the modulating source contribute mainly to the modulation of the occupation of the Mg-related energy level and only in a minor way to the modulation of the depletion layer edge. Above the defect transition frequency however, the hole response increases, remaining the only contribution to the junction capacitance.

Experimental studies of the electrical characteristics of Mg-doped GaN Schottky diodes have been reported in Refs.

[a]Electronic mail: m.schmeits@ulg.ac.be

13 and 14. Depletion region effects in GaN p–n junctions have been discussed by Kozodoy *et al.*[15]

The aim of this article is to present a theoretical study of the role of Mg in the electrical characteristics of GaN Schottky diodes, performing the detailed steady-state and small-signal analysis of a Schottky diode containing Mg-related deep acceptor levels. It starts from the numerical resolution of the basic coupled semiconductor equations, i.e., Poisson's equation and the continuity equations for electrons, holes and occupied impurity levels. This yields position-dependent values of the electrical potential, the energy band diagrams, the carrier concentrations, the current densities and the carrier recombination rates. As a final result, one obtains the electrical admittance Y, whose real part is the conductance G, and the imaginary part yields the total junction capacitance. This allows us to study in detail the influence of each microscopic parameter corresponding either to the material, the impurity, the junction, or the experimental conditions on the resulting macroscopic electrical quantities.

In the applications, we will determine the effect of the temperature T, the applied steady-state voltage and the series resistance. Finally, systems consisting of a double Schottky diode, i.e., two Schottky diodes connected back to back will be considered.

II. BASIC EQUATIONS AND NUMERICAL PROCEDURE

GaN is classified as a wide-gap semiconductor, with a room-temperature gap of 3.4 eV. Mg is giving rise to several impurity states with energies inside the gap. There is common agreement that there is one acceptor state whose energy position E_t is at 150–170 meV above the valence band edge.[7–9] In the numerical applications, we will take $E_t = 160$ meV for the activation energy. The total Mg concentration will be labeled N_t, with notations similar to those used for deep impurities.[16] Other eventually present shallow donor or acceptor concentrations are labeled N_D and N_A, respectively. The concentration of occupied defect levels for thermal equilibrium at temperature T is given by[17]

$$n_t = \frac{N_t}{1 + g \exp[(E_t - E_F)/kT]}, \tag{1}$$

where g is the degeneracy factor, k the Boltzmann constant, and E_F is the Fermi energy; g is assumed to equal 4, a value characteristic of acceptor levels.[17] The hole concentration p is given by

$$p = N_v \exp[(E_v - E_F)/kT], \tag{2}$$

where N_v is the effective valence band density of states. The electron concentration n can be expressed similarly. The equilibrium Fermi energy E_F is obtained by solving numerically the charge neutrality condition which writes for acceptor levels

$$p - n + N_D - N_A - n_t = 0. \tag{3}$$

The shallow dopants are supposed completely ionized. With a hole effective mass $m_h = 0.8\, m_0^7$, $N_t = 4 \times 10^{18}$ cm^{-3}, $N_D = 0$, and $N_A = 2 \times 10^{16}$ cm^{-3}, the thermal equilibrium values as function of temperature T of $(E_F - E_v)$, n_t, and p are given in Fig. 1. In this temperature range, the Fermi level is pinned at a value between the valence band edge E_v and the defect energy E_t. The equilibrium hole concentration is at least equal to N_A, increasing with temperature in a similar way to n_t. At room temperature (RT, $T = 293$ K), n_t reaches a value of 1.6×10^{17} cm^{-3}, which corresponds to about 4% of ionized acceptors.

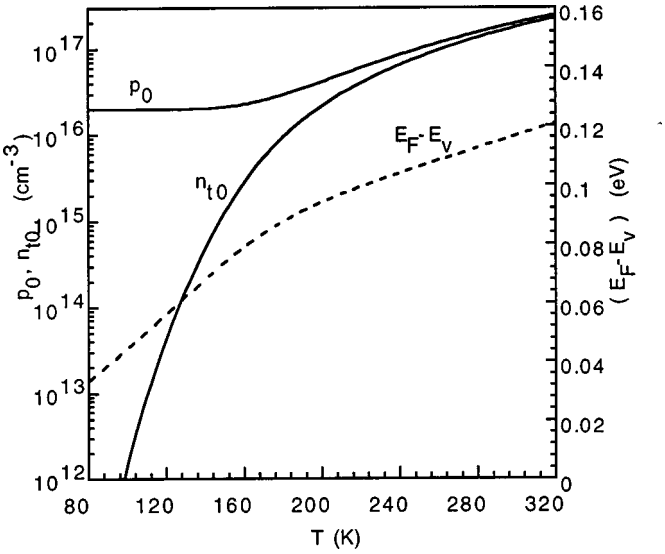

FIG. 1. GaN bulk Fermi level position in thermal equilibrium relative to the valence band edge, for $E_t - E_v = 0.16$ eV, $N_t = 4 \times 10^{18}$ cm^{-3}, and $N_A = 2 \times 10^{16}$ cm^{-3}. Steady-state bulk hole concentration p_0 and occupied Mg-level occupation n_{t0}, as function of temperature T.

The transition rates for electrons between the level E_t and the valence band are given according to the Shockley–Read–Hall[16] scheme by

$$r_{pt}(E_t) = c_p p n_t - e_p (N_t - n_t), \tag{4}$$

where c_p is the capture rate for holes, expressed in terms of the hole thermal velocity v_{th}^p and the hole thermal capture cross section σ_p by

$$c_p = v_{\text{th}}^p \sigma_p . \tag{5}$$

The thermal emission rate e_p is given by

$$e_p = \frac{c_p}{g} N_v \exp[(E_v - E_t)/kT]. \tag{6}$$

Similar expressions hold for the electron to conduction band transition rates r_{nt}. Carrier exchanges with the conduction band in this case plays only a minor role, as the defect energy position is close to the valence band edge. The electrical potential Ψ and the carrier concentrations n, p and n_t have to satisfy the basic semiconductor equations, namely Poisson's equation and the continuity equations for electrons, holes, and occupied defect levels.[18,19]

$$\nabla(\varepsilon \nabla \psi) = -q(p - n + N_D - N_A - n_t), \tag{7a}$$

$$\frac{\partial n}{\partial t} = \frac{1}{q} \nabla \cdot \mathbf{J}_n - r_{nt}, \tag{7b}$$

$$\frac{\partial p}{\partial t} = -\frac{1}{q}\nabla \cdot \mathbf{J}_p - r_{pt}, \tag{7c}$$

$$\frac{\partial n_t}{\partial t} = r_{nt} - r_{pt}, \tag{7d}$$

where $\mathbf{J}_n$ and $\mathbf{J}_p$ are, respectively, the electron and hole current densities

$$\mathbf{J}_n = n\mu_n \nabla E_c + \mu_n kT \nabla n, \tag{8a}$$

$$\mathbf{J}_p = p\mu_p \nabla E_v - \mu_p kT \nabla p, \tag{8b}$$

where μ_n and μ_p are the electron and hole mobilities, q is the electronic charge.

For the steady-state equations for a given value of temperature T and applied voltage V_0, the left-hand side of relations (7) is equal to zero. In the small signal analysis, the applied voltage contains in addition to the steady-state value V_0, a sinusoidally modulated term of frequency $f=\omega/2\pi$ and of amplitude $\tilde{V}$, small with respect to kT/q

$$V = V_0 + \tilde{V} e^{i\omega t}. \tag{9}$$

In the small-signal analysis, all quantities will have a dc component which will be given with an index '' 0'' and a harmonic component whose amplitude, labeled with a tilde, is complex in the general case. For example, the hole concentration writes

$$p(x,t) = p_0(x) + \tilde{p}(x)\, e^{i\omega t}. \tag{10}$$

Explicit expressions for the ac components are given in Ref. 20.

In the numerical study, the system is considered as one dimensional, with x giving the position. The position of the left boundary and right boundary of the region occupied by the semiconducting material are, respectively, x_L and x_R.

We place the Schottky contact at $x=x_L$. In the boundary conditions, the Schottky barrier height $q\phi_b$ is fixed. In thermal equilibrium it is related to the built-in potential V_{bi} and the bulk separation between the Fermi energy E_F and the depletion layer edge E_v by[17]

$$q\phi_b = qV_{bi} + (E_F - E_v). \tag{11}$$

In addition, a finite surface recombination velocity has to be given to fully characterize the metal–semiconductor contact.[18] At $x=x_R$, ohmic contact conditions are imposed when a single junction is considered. Some results will be given for back-to-back Schottky contacts, and in that case similar boundary conditions are imposed for both contacts.

Instead of using the variables Ψ, n, p, and n_t, the Eqs. (7a)–(7d) are expressed in terms of ψ and the quasi-Fermi energies F_n, F_p, and F_t, as these are more appropriate, giving variations of the same order of magnitude for the four unknowns. The set of Eqs. (7a)–(7d) is then solved numerically, after scaling and discretization according to a variable size mesh. As results one obtains the steady-state and small signal values of the electrical potential Ψ, the concentrations n, p, n_t, the recombination rates r_{nt} and r_{pt}, the current densities J_n and J_p and the displacement current J_D, in the ac case. The total ac current density $\tilde{J}$ is constant with respect to x. From its value, one obtains the admittance $Y = \tilde{J}/\tilde{V}$, from which the total capacitance C and conductance G can be obtained

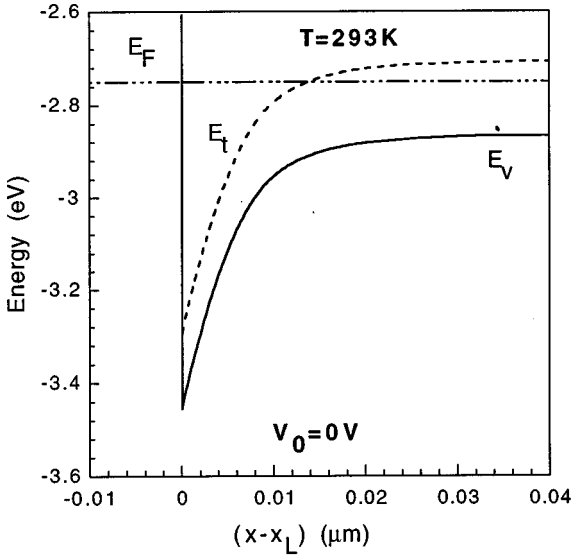

FIG. 2. Metal/GaN-p Schottky contact energy diagram for RT and zero-bias conditions. Mg acceptor level is at 0.16 eV above the valence band edge. Schottky barrier height is 0.7 eV. Left limit of semiconducting region is at $x_L=-10$ μm.

$$Y = G + i\omega C. \tag{12}$$

Both G and C depend on the frequency f, the steady-state voltage V_0, and the temperature T.

III. NUMERICAL RESULTS

A. Schottky GaN:Mg junction under room temperature, zero-bias conditions

We start by the study of a rectifying metal/GaN:Mg junction for which the chosen set of parameters corresponds to typical values resulting from experimental analysis.[7–9,21–24] The activation energy of the Mg acceptor level is taken at $(E_t - E_v) = 0.16$ eV. The Schottky barrier height $q\phi_b$ is taken 0.70 eV.[21–23] The hole surface recombination velocity is taken 10^9 cm/s. The deep and shallow dopant concentrations are, respectively, $N_t = 4\times10^{18}$ cm^{-3}, $N_A = 2\times10^{16}$ cm^{-3}. The total length of the device is chosen as 20 μm, such that series resistance effects are of moderate importance. The hole thermal cross section is $\sigma_p = 2\times10^{-20}$ cm^2;[24] and the hole mobility is $\mu_p = 10$ cm^2/V s[8]. The resulting energy band diagram for $T=293$ K and zero bias is given in Fig. 2. The bulk hole concentration is $p_0 = 1.8\times10^{17}$ cm^{-3} and represents a relatively strong effective doping, producing a depletion layer edge at 0.020 μm, this edge being not totally abrupt. The defect state crosses the equilibrium Fermi level at a distance of 0.014 μm from the left metal/semiconductor interface.

In Fig. 3, we represent for the same conditions, the steady-state concentrations $n_{t0}(x)$ and $p_0(x)$ as function of position x, together with the absolute values of the small-signal amplitudes $\tilde{n}_t(x)$ and $\tilde{p}(x)$. The latter have been calculated for three different frequencies [low (LF), medium

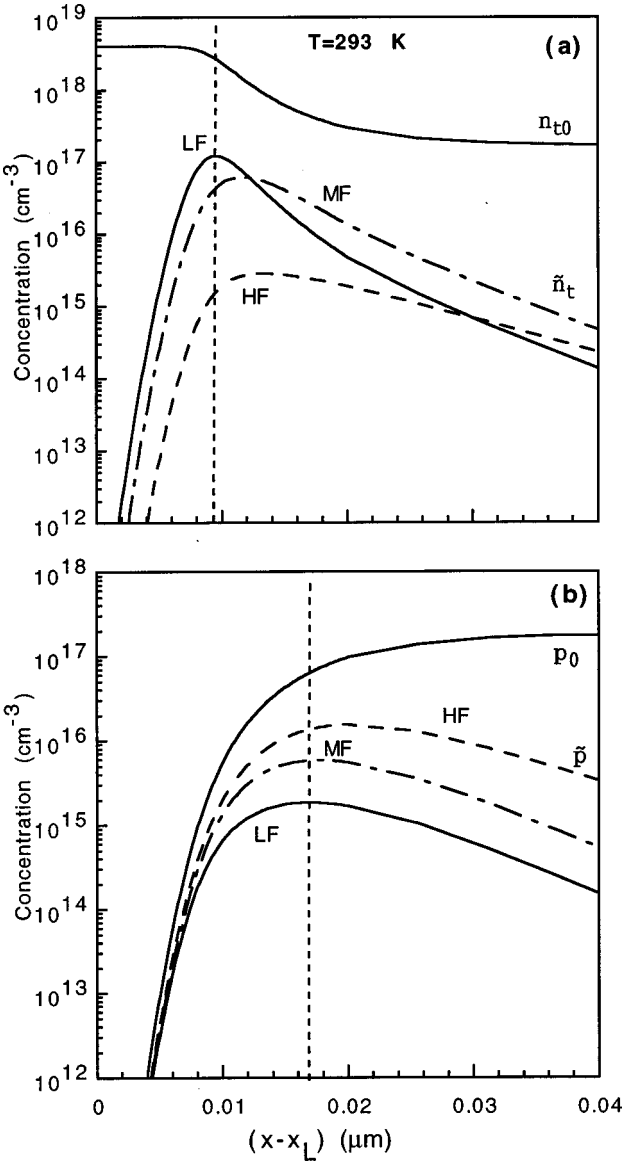

FIG. 3. Steady-state impurity concentration n_{t0} and hole concentration p_0, as function of position x, for RT and zero-bias conditions. Absolute value of small-signal ac amplitude for three frequencies of the applied ac voltage $f=10^2$ Hz (LF), $f=5\times10^3$ Hz (MF), $f=10^5$ Hz (HF).

(MF), and high(HF)], $f=10^2$ Hz (LF), 3×10^3 Hz (MF), and 10^5 Hz (HF), the notations used becoming clear in the following. At low frequency, this absolute value is practically equal to the real part $\tilde{n}_t^R$, changed by sign. Having chosen the voltage amplitude $\tilde{V}$ real, $\tilde{n}_t^R$ is negative. At low frequency, $\tilde{n}_t(x)$ presents a peak at a distance of 0.01 μm from the junction, a position where $n_{t0}(x)$ is at about 50% of its maximum value; $\tilde{p}(x)$ presents its maximum value at 0.017 μm from the left boundary. These responses remain approximately constant up to 5×10^2 Hz, i.e., as long as the impurity states are able to completely follow the variations of the applied voltage. With increasing modulation frequency, the amplitude $\tilde{n}_t(x)$ decreases as expected, reaching at the HF frequency a value reduced by about a factor 10^2 with respect to the low frequency value. The variation of $\tilde{p}(x)$ with frequency is however different. It does not simply remain constant above the impurity transition frequency, but increases above the MF frequency, reaching in the HF regime a value which is by a factor of 10 larger than the LF value.

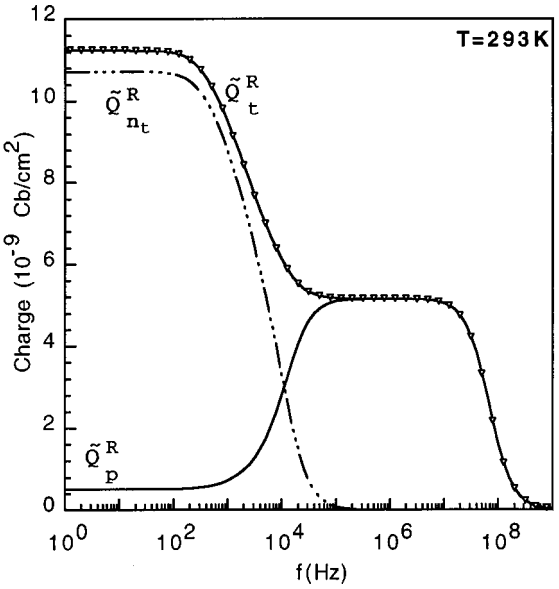

FIG. 4. Integrated absolute value of the real part amplitude of the ac response of $q\tilde{n}_t$, $q\tilde{p}$, $q(\tilde{n}_t-\tilde{p})$.

The same behavior is illustrated in Fig. 4, where one shows, as function of frequency, the real part of the charges related to the amplitude of the impurity level concentration, hole concentration, and charge density. These are defined as

$$\tilde{Q}^R_{n_t}=q\int_{x_L}^{0}|\tilde{n}_t^R|\,dx, \tag{13a}$$

$$\tilde{Q}^R_p=q\int_{x_L}^{0}\tilde{p}^R(x)\,dx, \tag{13b}$$

$$\tilde{Q}^R_t=q\int_{x_L}^{0}(\tilde{p}^R-\tilde{n}_t^R)\,dx. \tag{13c}$$

The upper limit of the integration given here is largely above the x values where the integrands are of negligible value; $x=0$ represents here $(X_R-X_L)/2$.

These curves show that the modulated space charge contribution due to the exchange of carriers between the Mg-related impurity level and the valence band goes to zero at a transition frequency of 4×10^3 Hz. At the same time, as the impurity response decreases, the response of the holes at the depletion layer edge increases, keeping a constant value up to 10^7 Hz. Above this value, the hole response goes to zero with a cutoff frequency corresponding, in electrical terms, to the *RC* cutoff frequency of a *RC* series circuit, where *C* is the depletion-layer capacitance and *R* the series resistance. The modulation of the total charge $\tilde{Q}_t^R$ is the resulting sum of both contributions, where the LF contribution is due essentially to the response of the impurity level and the HF contribution is due essentially to the holes modulating the depletion layer edge. The LF contribution of the holes exists in this case, because a nonzero value of the shallow acceptor concentration N_A has been assumed. Without this term, $\tilde{Q}_p^R$

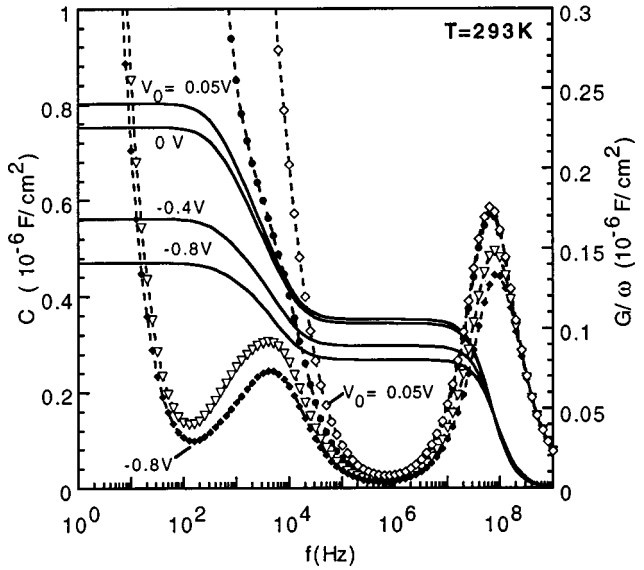

FIG. 5. Capacitance per unit section C and conductance per unit section G over ω, as function of frequency f for RT conditions, for metal /GaN:Mg junction with applied steady-state voltages $V_0 = +0.05$, 0, -0.4, and -0.08 V. Length of the structure is $(x_R - x_L) = 20$ μm. Hole mobility is $\mu_h = 10$ cm^2/V s.

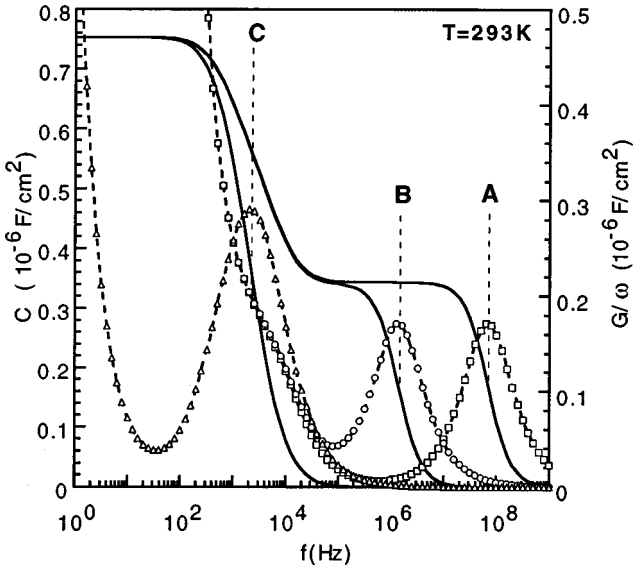

FIG. 6. Capacitance per unit section C and conductance per unit section G over ω, of Schottky junction with parameters of Fig. 5, (curve A), length multiplied by factor 50 (curve B), length multiplied by factor 50, and mobility divided by factor 200 (curve C).

would have been zero in the LF case. Dividing $\tilde{Q}_t^R$ by the amplitude of the ac voltage yields $\tilde{V}$ yields nothing but the capacitance of the whole structure.

This behavior is obviously different from that of p–n junctions or Schottky diodes containing shallow, fully ionized dopants and deep impurities, with concentrations of the shallow dopants larger than those of the impurities.[10–12] Here the hole (or electron) response resulting from the modulation of the depletion layer edge remains constant over the entire frequency range, yielding a constant (called HF) capacitance term. The contribution of the impurity level exchanging carriers with the valence (or conduction) band gives an additional contribution from zero frequency up to the transition frequency where the impurity levels no longer respond to the applied voltage. Here, the Mg level acts simultaneously as dopant and deep impurity. Depending on frequency, there is a competition between the two functions. In the LF range, the holes provided by the modulating voltage source essentially modify the charge on the impurity level. When these are no longer able to follow the applied voltage modulation, the holes contribute to the modulation of the depletion layer charge, but with a stronger amplitude than in the LF regime.

B. Effect of applied steady-state voltage V_0

In Fig. 5, we show as a function of frequency and for different values of the steady-state voltage V_0 the resulting variations of the capacitance C and of G/ω. The curve of G/ω presents a peak at the cutoff frequencies of the capacitance, or at least a shoulder when the conductance G is too large. As the reverse voltage increases, the capacitance decreases both in the LF and the HF regimes. The plot of the inverse square values of C_{LF} and C_{HF} as function of V_0 yields, within the particular values if the parameters we have used, a straight line. However, care should be taken before directly applying textbook relations in order to determine dopant concentrations or built-in voltages.

C. Effect of series resistance

The series resistance in a structure depends on the distance separating the ohmic contact from the depletion layer edge, in our case this is essentially $(x_L - x_R)$. It also depends on the geometry of the structure, which in many cases has not a linear configuration. Gallium nitride is often grown on a sapphire substrate, on which it is impossible to realize contacts of either ohmic or Schottky type. The contacts are therefore evaporated on top of the GaN layer.

We have considered different cases, simulating these effects. In Fig. 6, curve (A) corresponds to the previously treated case, with $l = (x_L - x_R) = 20$ μm and $\mu_p = 10$ cm^2/V s. For curve (B), the length is taken $l = 1000$ μm, all other parameters remaining constant. This causes a shift of the *RC* cutoff frequency by a factor 50, the rest of the *C(f)* curve is unmodified. For curve (*C*), the hole mobility of GaN outside the depletion region has been divided by a factor 200. In a one-dimensional analysis, cylindrical symmetry along the x axis is implicit. The reduction of the mobility would simulate a three-dimensional structure where the conduction channel has a cross section much smaller than the metallic contacts. This is, for example, the case in a planar structure where contacts of about 1 mm^2 section are realized on a GaN layer whose thickness is in the micrometer range. In this case, as seen on curve (*C*), the *RC* cutoff frequency has moved below the impurity transition frequency. The new cutoff frequency of 2×10^3 Hz corresponds to the *RC* cutoff frequency, where R is still the series resistance R_s and C is now the LF capacitance, due essentially to the response of the impurity level. The electrical character governs the response of the system, irrespective of the microscopic origin of the capacitance. It

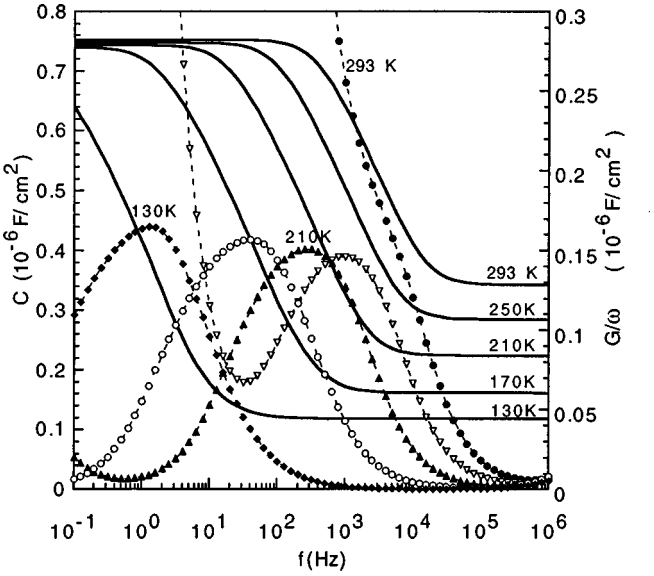

FIG. 7. Capacitance per unit section and G/ω per unit section as function of frequency f for Schottky metal/GaN:Mg junction at different temperatures T=293, 250, 210, 170, and 130 K.

should be mentioned that the low frequency value of the capacitance remains unmodified by the change in series resistance, as this latter produces no modifications in the region where the occupation of the impurity level changes.

D. Effect of temperature

Modifying the temperature is expected to produce effects at several levels. It modifies the position of the equilibrium Fermi level E_F relative to the valence band edge. The value of the energy gap and of the impurity activation energy are assumed to remain constant with T. Temperature also affects the occupation of the Mg level and the hole equilibrium concentration in the valence band, as well as the thermal transition rates r_{pt}. In Fig. 7, we show the C–f and G/ω curves for temperatures T=293, 250, 210, 170, and 130 K. The low frequency capacitance remains nearly constant with temperature, whereas the HF capacitance decreases with T. This latter effect is clearly a consequence of the reduction of the hole concentration in the valence band. The transition frequency f_t between the LF and the HF values decreases with temperature. Assuming this frequency equal to the thermal emission rate e_p, divided by 2π, would give a temperature dependence of the type

$$f_t \propto T^2 \exp(-\Delta E^*/kT), \tag{14}$$

where ΔE^* should be in principle equal to $(E_t - E_v)$, the impurity ionization energy. A plot of the numerically obtained transition frequencies as function of $1/kT$ yields, in our particular case, a value of $\Delta E^* = 0.115$ eV, which is less than the used value of $(E_t - E_v) = 0.160$ eV. By writing $f_t = e_p/2\pi$, several terms are neglected already in the classical case.[25] In addition, the original relation has been established in a context which is not fully realized in the case treated here. It effectively assumes a concentration of fully ionized shallow dopants, with a concentration larger than the deep impurity concentration and both entities being of a distinct nature.

IV. BACK-TO-BACK CONNECTED SCHOTTKY DIODES

In experimental situations, one may meet configurations where the electrical measurements are performed on samples with two identical contacts, which both are of Schottky type. In that case, it is necessary to describe both contacts as Schottky junctions. In the numerical treatment used here, this presents no major difficulty, as it needs only to set the appropriate boundary conditions on the second contact.

In the case of a symmetric double Schottky diode, with homogeneous doping and impurity concentrations and with the same value of the Schottky barrier height $q\phi_b = 0.70$ eV at the left and right contact, the resulting amplitudes of the carrier concentrations are antisymmetric with respect to the center of the structure $x=0$. This is illustrated in Fig. 8 where we show the real part of $\tilde{n}_t$, for x values close to both semiconductor/metal interfaces. The resulting capacitance–frequency curves for the $V_0 = 0$ case have the same shape than those shown in Fig. 3, except that all values are divided by a factor of about 2, as in that case the voltage is applied to a system which consists essentially of two identical diodes placed in series.

In order to study the effect of the asymmetry of the contacts, we have treated two other cases, where the Schottky barrier height has been kept equal to $q\phi_b = 0.70$ eV at the left contact, but set equal to respectively 0.50 and 0.90 eV on the right contact. This leads to completely different ac-impurity occupation functions in the two sides of the structure. As shown in Fig. 8, the amplitude of $\tilde{n}_t^R$ is strongest on the side where the Schottky barrier is largest. The weakest barrier seems to have a behavior similar to that of an ohmic contact. This feature is illustrated in Fig. 9, where we show for the case where $q\phi_b = 0.90$ eV at the right contact, the values of the integrated real parts of the carrier amplitudes. The integrations are performed on x values close to the respective contacts. The resulting functions are drastically different from those shown in Fig. 4. The low frequency part of the modulated space charge has now two contributions, one from the right contact, below 10^4 Hz, and one from the left contact, centered at 5×10^2 Hz. The HF contribution of the holes is of equal importance on both sides of the structure. Taking the resulting total charge amplitudes $\tilde{Q}_t^R$ divided by $\tilde{V}$ here does not give the capacitances of the isolated junctions, as can be seen by comparing the result for the left contact with that shown in Fig. 4.

The resulting C–f and G/ω curves for the three cases are shown in Fig. 10. The cutoff at 10^8 Hz remains unmodified by the height of the barriers. The low frequency capacitance is larger for the two asymmetric structures, compared to the symmetrical one. the marked feature introduced by the asymmetry is to produce a new peak in the G/ω curves, to which new steps in the C–f characteristics correspond. In the case where the right barrier has been reduced (curve b), the peak in G/ω appears at 5×10^5 Hz, i.e., beyond the former transi-

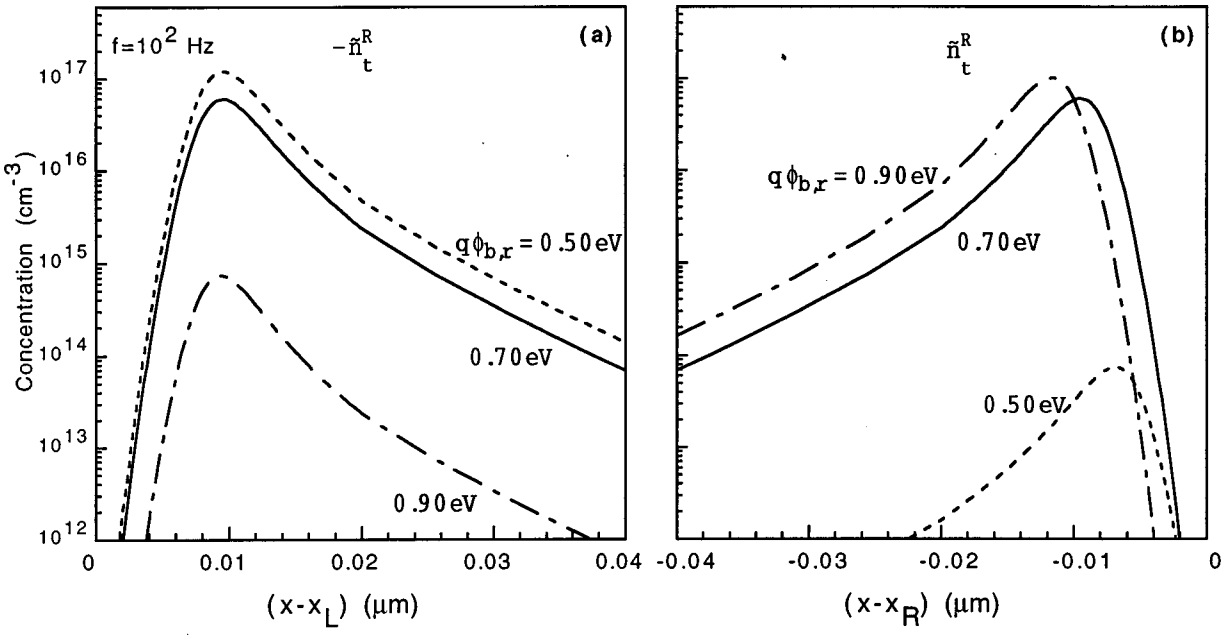

FIG. 8. ac response at $f=100$ Hz of real part of occupied impurity concentration for back-to back connected Schottky diodes. For left contact, minus real part is shown. Schottky barrier height for left contact is 0.70 eV. Barrier heights for right contacts are, respectively, 0.70, 0.50, and 0.90 eV.

tion frequency. It is due to an enhanced hole response in that frequency range. In the case of on enhanced barrier height (curve c), the new peak is at 10^2 Hz, due this time to a modified impurity level response.

These features can be retrieved in the study of an equivalent lumped electrical circuit composed of two different *RC* circuits in parallel, placed in series with a resistance R_s. Each *RC* circuit represents a junction. Taking different values of the resistances R_1 and R_2 and the capacitances C_1 and C_2 produces the appearance of cutoff frequencies in the equivalent total capacitance and conductance, which are not present in a symmetrical structure.

V. CONCLUSIONS

We have investigated the role of the deep dopant magnesium in the electrical characteristics of GaN Schottky diodes. From our theoretical analysis it can be concluded that Mg acts neither as a simple deep impurity, nor as a classical shallow dopant. Mg has both behaviors, but not in a simple

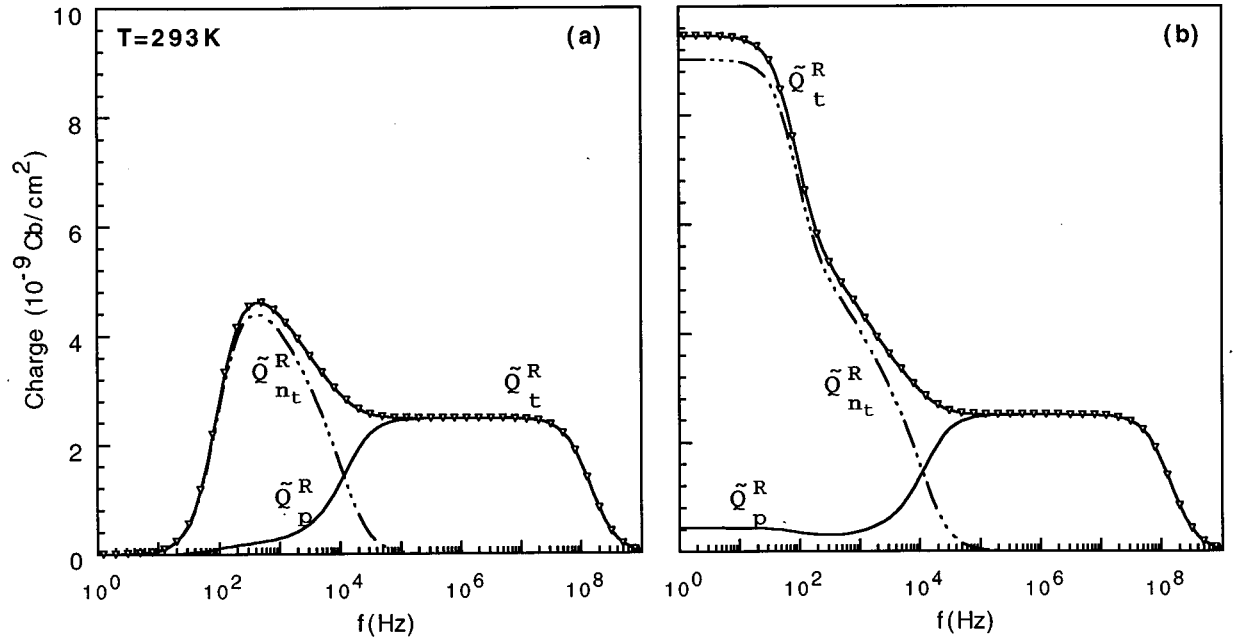

FIG. 9. Integrated absolute value of the real part amplitude of the ac response of $q\,\tilde{n}_t$, $q\,\tilde{p}$, $q(\tilde{n}_t-\tilde{p})$ of back-to-back connected Schottky diode, for left contact and for right contact, in case of left Schottky barrier height of 0.70 eV and of right Schottky barrier height of 0.90 eV.

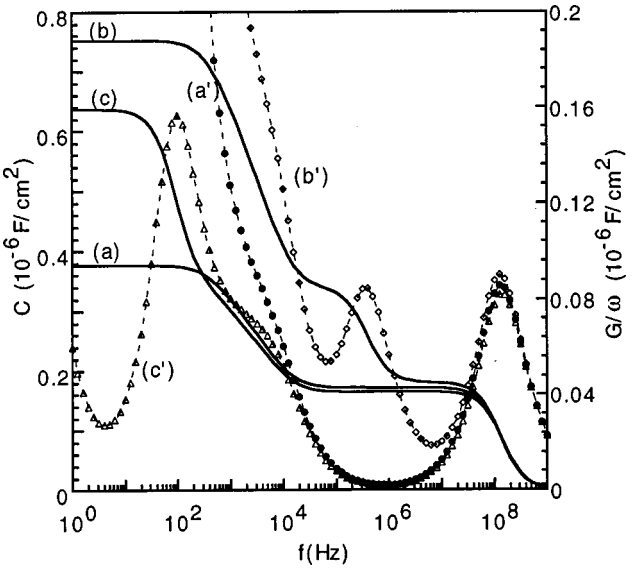

FIG. 10. Capacitance per unit section and G/ω per unit section as function of frequency f for back-to-back connected Schottky contacts. Left Schottky barrier height is 0.70 eV, right Schottky barrier height is, respectively, 0.70 eV (curves a,a′), 0.50 eV (curves b,b′) and 0.90 eV (curves c,c′).

additive way. There is effectively a competition between the deep impurity character and the dopant character. At low frequency, the electrical characteristics are determined by the impurity behavior; above the defect transition frequency, the hole modulation at the depletion layer edge dominates. These conclusions could only be obtained through the used numerical study, which gives results which are quantitatively reliable. No approximations are made, once the basic equations are formulated.

We have studied in detail the effect of parameters which may be varied in a complete experimental study, namely the applied steady-state voltage, the temperature, and the series resistance. Results for the effect of asymmetry in a double-Schottky diode configuration are also given and show the appearance of new features in the electrical characteristics.

ACKNOWLEDGMENTS

Financial support by the Belgian Fonds National de la Recherche Scientifique (Contract No. 9.4565.96F) and by an INTAS Grant No. N97-0995 are gratefully acknowledged.

[1] J. Y. Duboz, Phys. Status Solidi A **176**, 5 (1999).
[2] S. Nakamura, T. Mukai, and M. Senoh, Appl. Phys. Lett. **64**, 28 (1994).
[3] M. Asif Khan, J. N. Kuznia, D. T. Olson, M. Blasingame, and A. R. Bhattarai, Appl. Phys. Lett. **63**, 2455 (1993).
[4] E. Monroy, M. Hamilton, D. Walker, P. Kung, F. J. Sanchez, and M. Razeghi, Appl. Phys. Lett. **74**, 1171 (1999).
[5] C. Zolper, R. J. Shul, A. G. Baca, R. G. Wilson, S. J. Pearton, and R. A. Stall, Appl. Phys. Lett. **68**, 2273 (1996).
[6] J. I. Pankove, M. Leksono, S. S. Chang, C. Walker, and B. Van Zeghbroeck, MRS Internet J. Nitride Semicond. Res. **1**, 39 (1996).
[7] T. Tanaka, A. Watanabe, H. Amano, Y. Kobayashi, I. Akasaki, S. Yamazaki, and M. Koike, Appl. Phys. Lett. **65**, 593 (1994).
[8] H. Nakayama, P. Hacke, M. R. H. Khan, T. Detchprohm, K. Hiramatsu, and N. Sawaki, Jpn. J. Appl. Phys., Part 2 **35**, L282 (1996).
[9] W. Götz, N. M. Johnson, J. Walker, D. P. Bour, and R. A. Street, Appl. Phys. Lett. **68**, 667 (1996).
[10] W. G. Oldham and S. K. Naik, Solid-State Electron. **15**, 1085 (1972).
[11] Y. Zotha, Solid-State Electron. **16**, 1029 (1973).
[12] M. Beguwala and C. R. Crowell, Solid-State Electron. **17**, 203 (1974).
[13] J. W. Huang, F. T. Kuech, H. Lu, and I. Bhat, Appl. Phys. Lett. **68**, 2392 (1996).
[14] Y. Zotha, H. Kuroda, R. Nii, and S. Nakamura, J. Cryst. Growth **189/190**, 616 (1998).
[15] P. Kozodoy, S. P. Den Baars, and U. K. Mishra, J. Appl. Phys. **87**, 770 (2000).
[16] M. Schmeits, M. Sakhaf, and S. Munnix, J. Appl. Phys. **74**, 6266 (1993).
[17] S. M. Sze, *Physics of Semiconductor Devices* (Wiley, New York, 1981).
[18] S. Selberherr, *Analysis and Simulation of Semiconductor Devices* (Springer, Wien, 1984).
[19] C. M. Snowden, *Semiconductor Device Modelling* (Peter Peregrinus, London, 1988).
[20] M. Sakhaf and M. Schmeits, J. Appl. Phys. **80**, 6839 (1996).
[21] T. Mori, T. Kozawa, T. Ohwaki, Y. Taga, S. Nagai, S. Yamasaki, S. Asami, N. Shibata, and M. Koike, Appl. Phys. Lett. **69**, 3537 (1996).
[22] H. Harima, T. Inoue, S. Nakashima, K. Furukawa, and M. Taneya, Appl. Phys. Lett. **73**, 2000 (1998).
[23] X. A. Cao, S. J. Parton, G. Dang, F. P. Zhang, F. Ren, and J. M. Van Hove, Appl. Phys. Lett. **75**, 4130 (1999).
[24] D. J. Kim, D. Y. Ryu, N. A. Bojarczuk, J. Karasinski, S. Guha, S. H. Lee, and J. H. Lee, J. Appl. Phys. **88**, 2564 (2000).
[25] See, e.g., Ref. 10, relations (19).